Bioinspired ultrasound-responsive piezoelectric topological patches with controlled magnesium release and immunomodulation for bone defect repair

Zhengwei Liu[a b], Hui Zhang[c], Yu Wang[c d] *, Yuanjin Zhao[c] *, Yongxiang Wang[a b] *

[a] Department of Orthopedics, Northern Jiangsu People's Hospital, 225001, Yangzhou, China.

[b] Department of Orthopedics, Northern Jiangsu People's Hospital, Clinical Teaching Hospital of Medical School, Nanjing University, 225001, Yangzhou, China

[c] Department of Rheumatology and Immunology, Nanjing Drum Tower Hospital, School of Biological Science and Medical Engineering, Southeast University, 210096, Nanjing, China.

[d] Zhejiang Key Laboratory of Soft Matter Biomedical Materials, Wenzhou Institute, University of Chinese Academy of Sciences, Wenzhou, Zhejiang 325000, China.

*Corresponding author. Email: yuwang@wiucas.ac.cn (Y. Wang); yjzhao@seu.edu.cn (Y.J. Zhao); wangyongxiang@nju.edu.cn (Y.X. Wang)

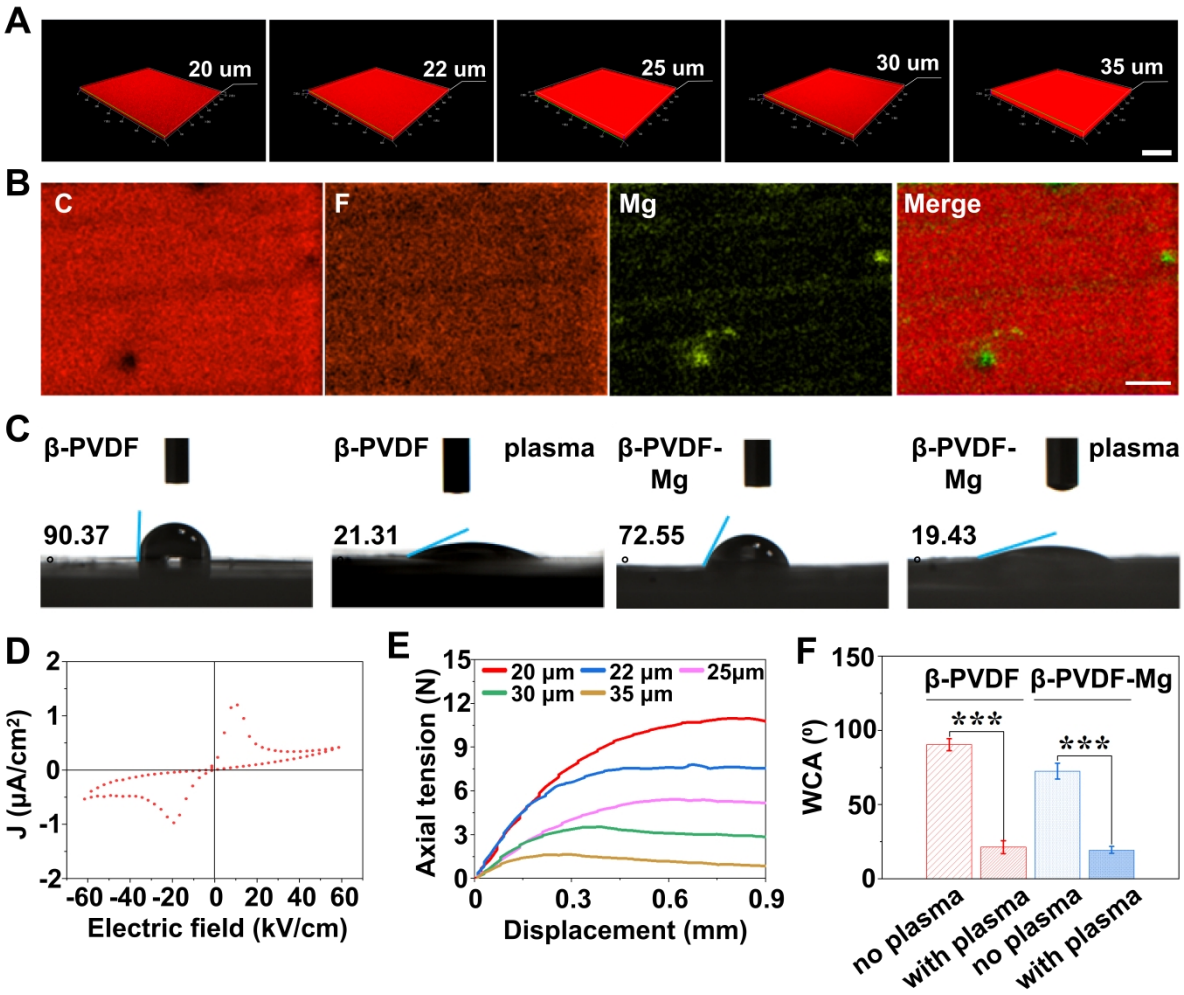


Figure S1. Characterization of the β-PVDF-Mg patches. (A) Three-dimensional confocal microscopy images of β-PVDF-Mg patches with varying thickness; scale bar: 100 μm. **(B)** EDS picture of β-PVDF-Mg patch; scale bar: 5 μm. **(C)** Water contact angles of β-PVDF and β-PVDF-Mg patches before and after oxygen plasma treatment (60 W, 3 min, O_2 flow rate 200 mL/min). **(D)** Leakage current analysis of β-PVDF-Mg patch. **(E)** Typical stress-strain curves of β-PVDF-Mg patch. **(F)** Quantitative statistical analysis of WCA values across samples (n = 3 for each group). Data are mean ± SD from three biologically independent replicates; one-way ANOVA: ***$p < 0.001$.

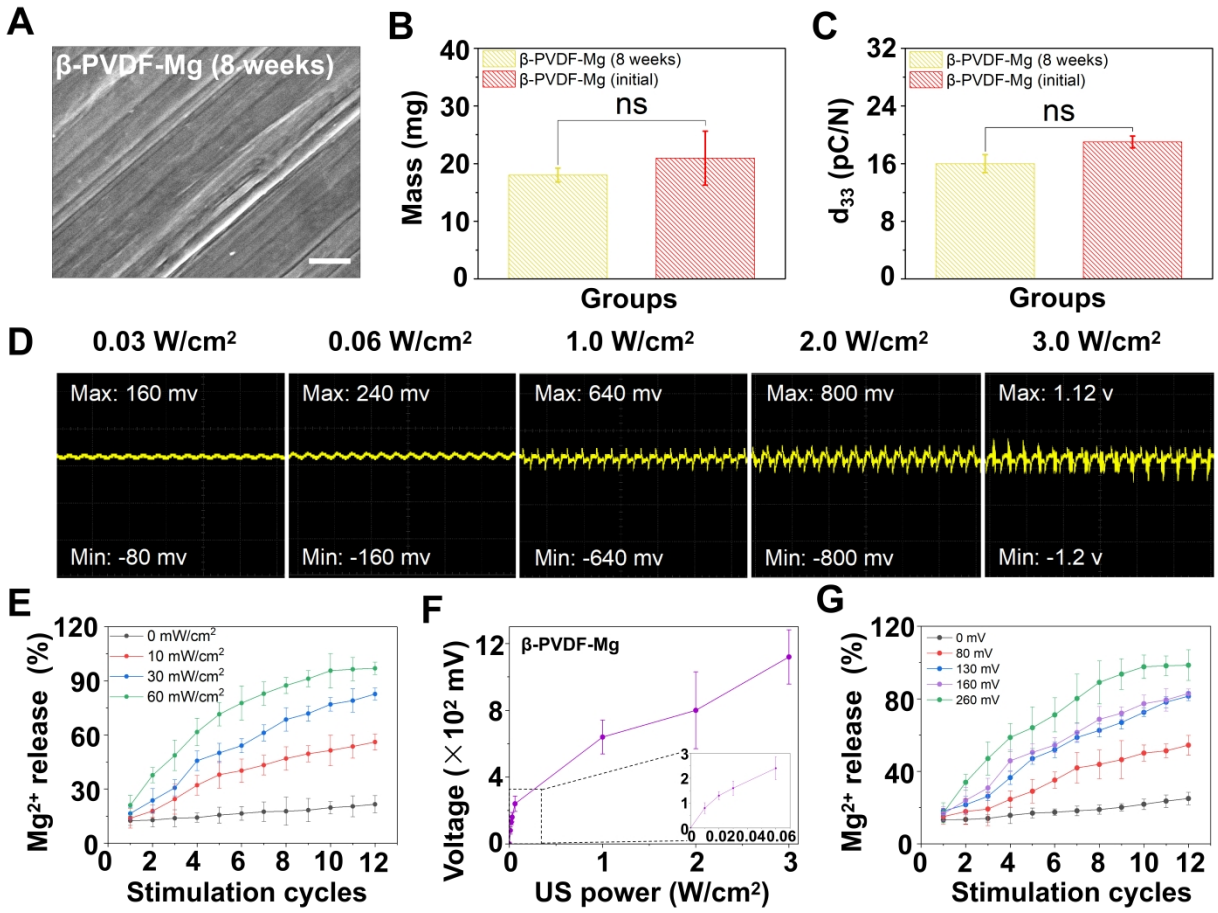


Figure S2. Characterization of the β-PVDF-Mg patches. (A) SEM picture of β-PVDF-Mg patch after 8 weeks *in vivo;* scale bar: 2 μm. **(B)** The mass of the β-PVDF-Mg patch after 8 weeks *in vivo* and the initial β-PVDF-Mg patch, separately. **(C)** The d_{33} constant of the β-PVDF-Mg patch after 8 weeks *in vivo* and the initial β-PVDF-Mg patch, separately. **(D)** Voltage values of β-PVDF-Mg patch during US stimulation with different power after 8 weeks *in vivo*. **(E)** The cumulative release percentage of Mg^{2+} from β-PVDF-Mg patch during US stimulation with different power (n = 3). **(F)** The voltage generated by the β-PVDF-Mg patch during US stimulation with different power (n = 3). **(G)** The cumulative release percentage of Mg^{2+} from β-PVDF-Mg patch under different output voltages (n = 3). Data are mean ± SD from three biologically independent replicates; one-way ANOVA: ns, not significant.

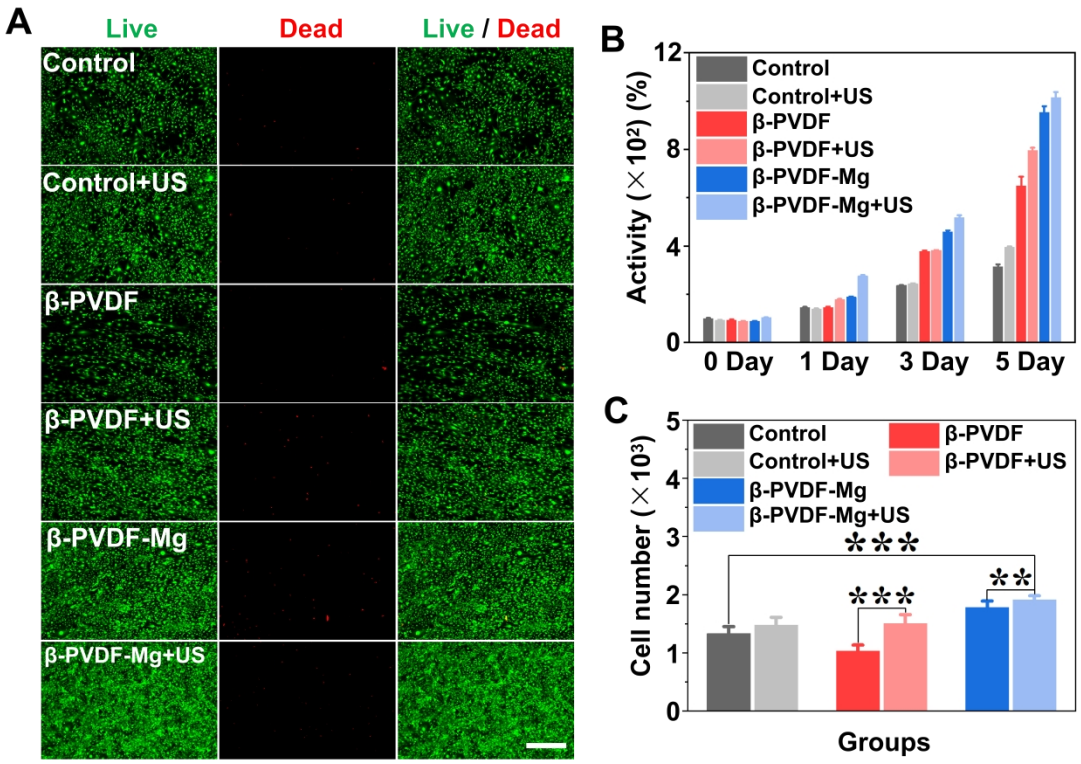


Figure S3. Cell proliferation and viability assessment. (A) Biocompatibility picture of MC3T3-E1; scale bar: 100 μm. **(B, C)** CCK-8 assay results for MC3T3-E1 (n = 5). Data are mean ± SD from five biologically independent replicates; one-way ANOVA: $^{**}p < 0.01$, $^{***}p < 0.001$.

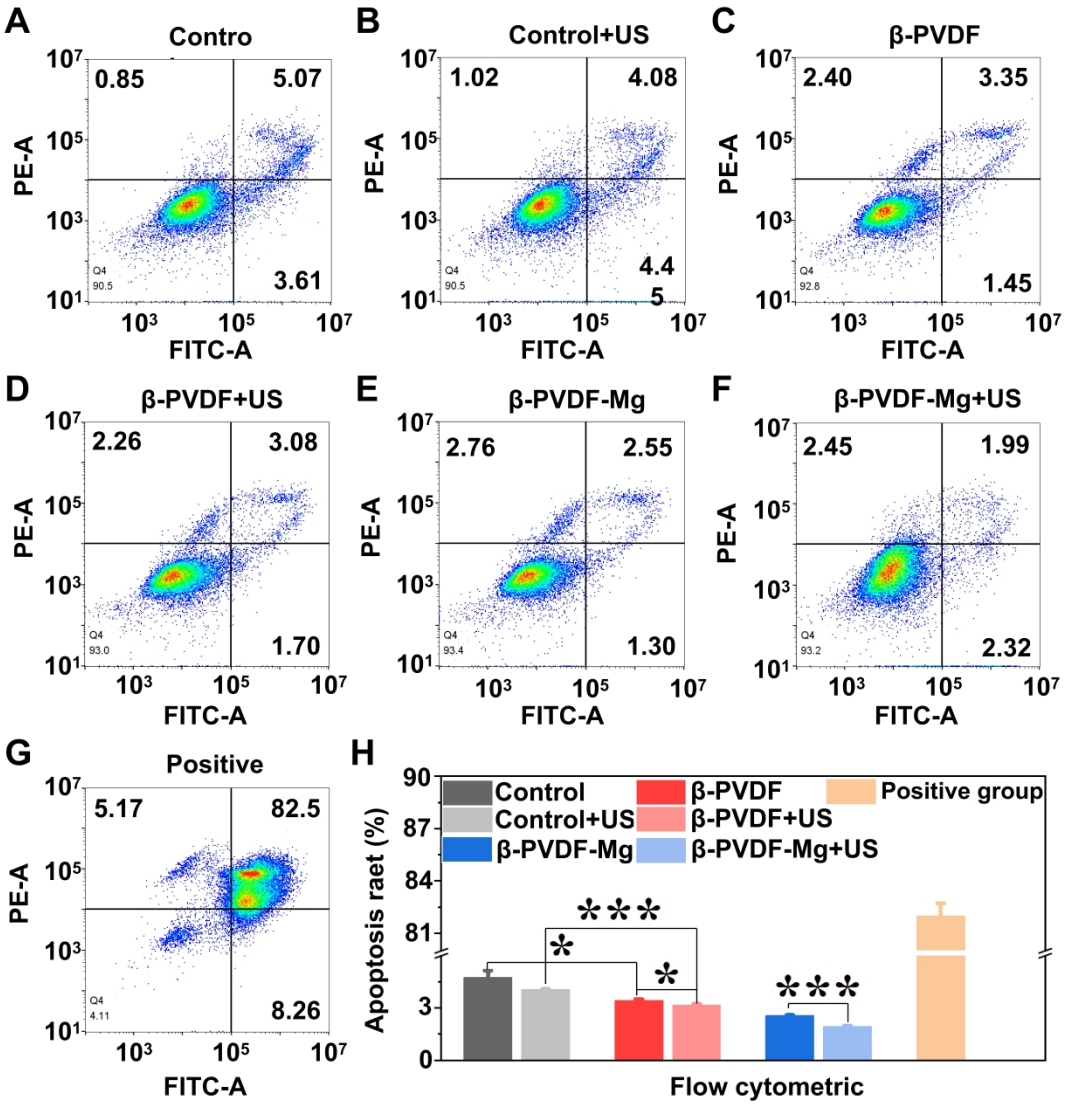


Figure S4. Analysis of cell apoptosis. (A-G) Flow cytometry results showing apoptosis of MC3T3-E1 in each group (n = 3). **(H)** Statistical analysis of apoptotic MC3T3-E1. Data are mean ± SD from three biologically independent replicates; one-way ANOVA: *$p < 0.05$, ***$p < 0.001$.

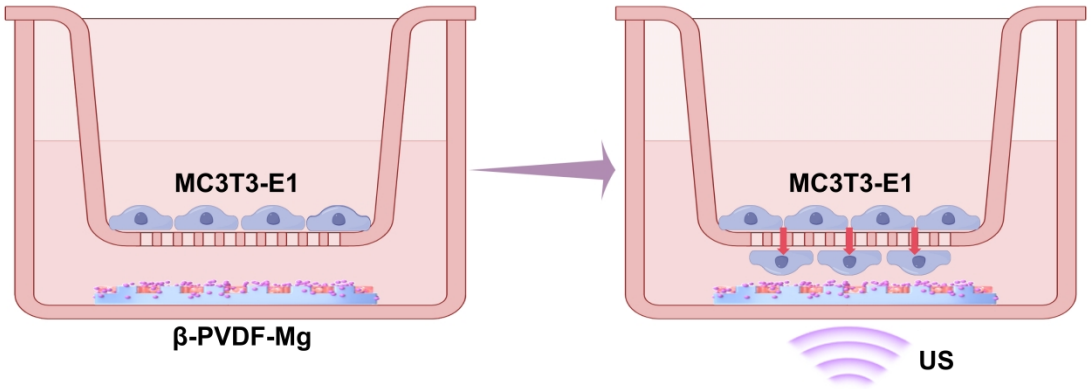


Figure S5. Schematic illustration of Transwell assay for MC3T3-E1 recruitment *in vitro*.

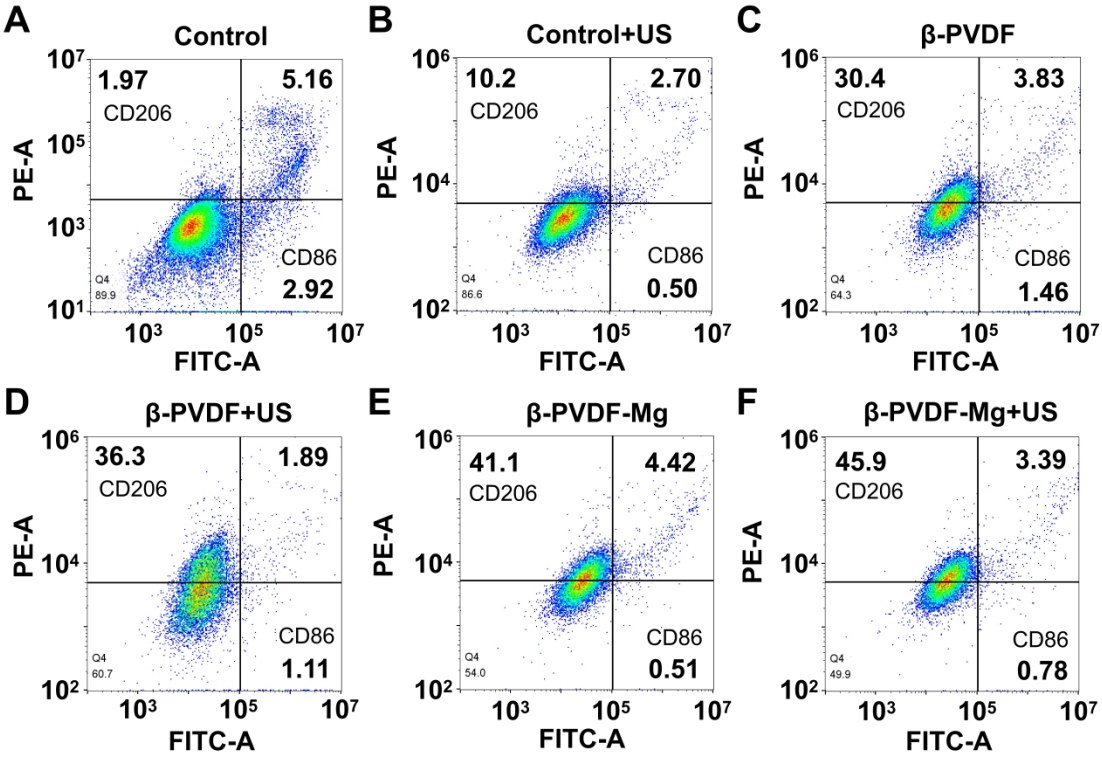


Figure S6. Immunomodulation of β-PVDF-Mg patches. (A-F) Flow cytometric analysis of M1 and M2 polarization in RAW264.7 cells from each group (n = 3). Three biologically independent replicates were performed.

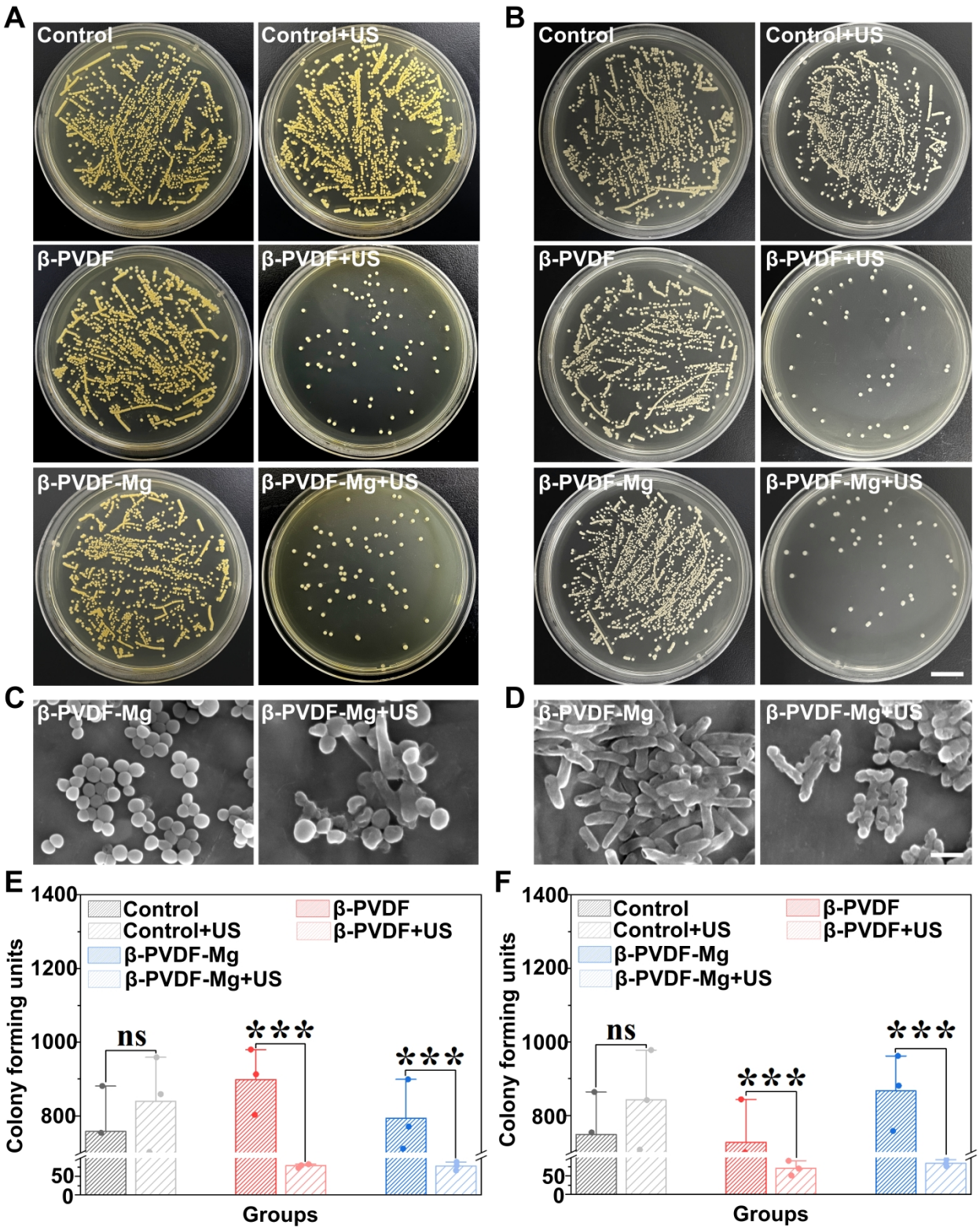


Figure S7. Preliminary antibacterial response of β-PVDF-Mg to US stimulation. (A, B) Colony formation of *S. aureus* and *E. coli* following the indicated treatments; scale bar: 14 mm. **(C, D)** SEM

analysis of bacterial morphological changes under US and non-US conditions; scale bar: 0.5 μm. **(E, F)** Quantification of viable colonies (n = 3). Values represent the mean ± SD of three biologically independent experiments. Statistical comparisons were performed using one-way ANOVA followed by Tukey's multiple-comparison test, with ***p < 0.001; ns, not significant.

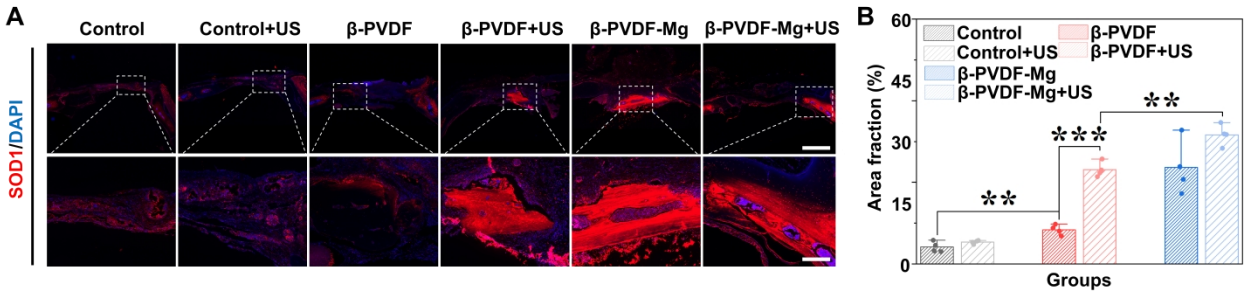


Figure S8. IF staining of SOD1. (A) IF staining of SOD1; scale bars: 1.5 mm (top) and 100 μm (bottom). **(B)** Statistical analysis of SOD1 (n = 4). Data are mean ± SD from four biologically independent replicates; one-way ANOVA: **p < 0.01, ***p < 0.001.

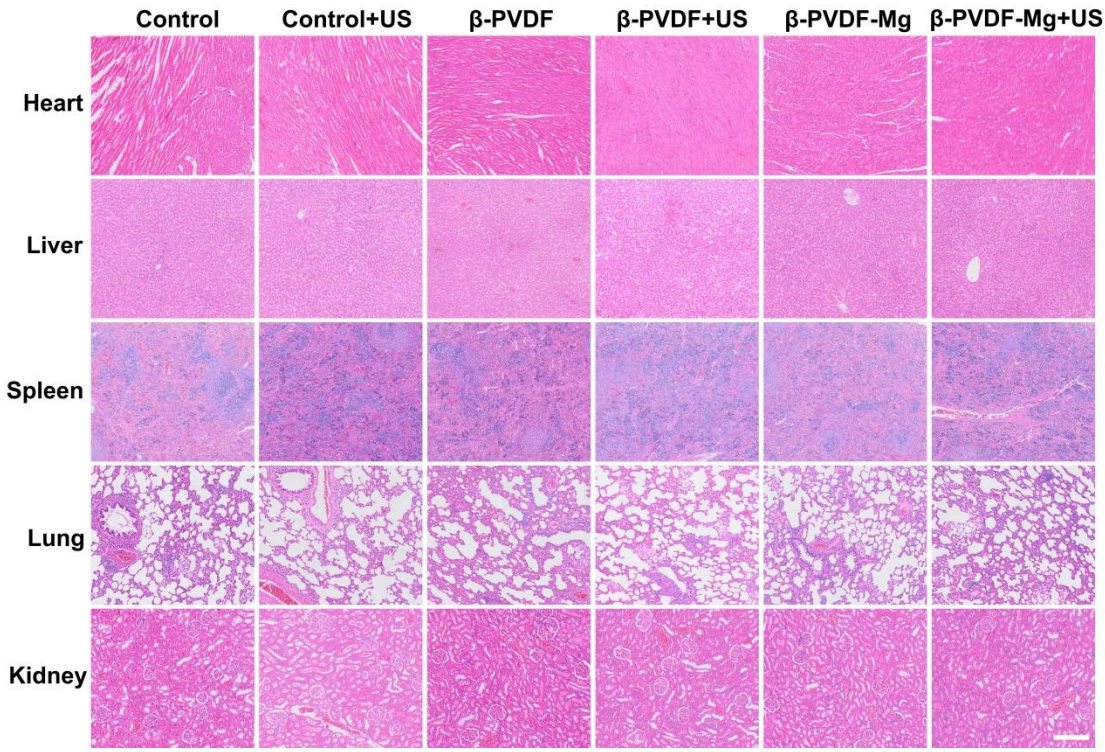


Figure S9. Histological evaluation of major organs after 8 weeks of implantation. H&E-staining picture from rats in the Control, Control+US, β-PVDF, β-PVDF+US, β-PVDF-Mg, and β-PVDF-Mg+US groups; scale bar: 200 μm. n = 4 rats per group. Four biologically independent replicates were performed.

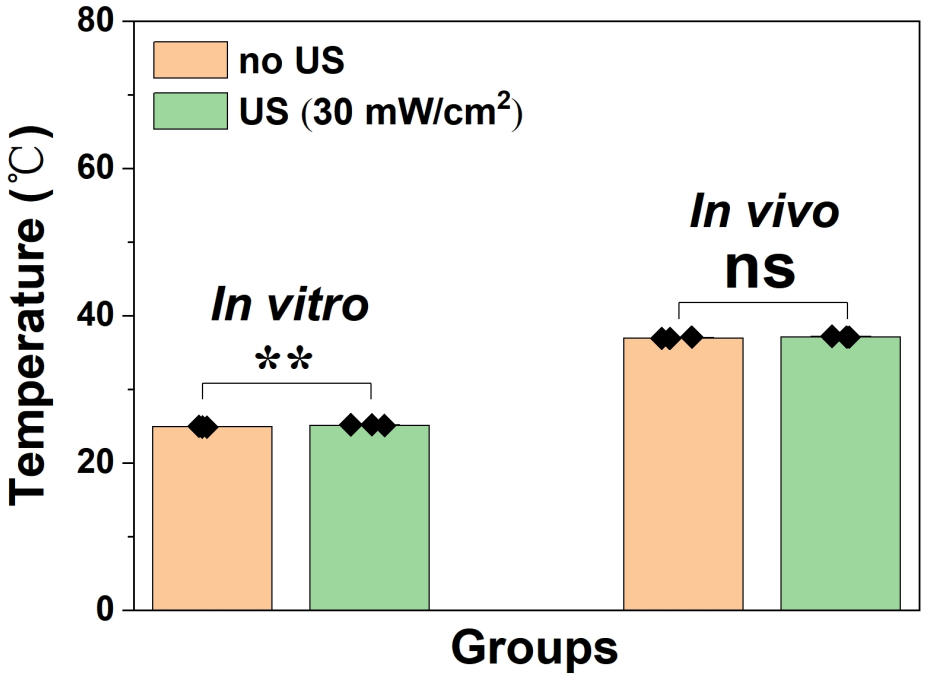


Figure S10. Thermal effect of US. No appreciable bulk temperature increase was observed during the 20 min LIPUS exposure, suggesting that the observed biological effects were unlikely to be primarily attributable to US-induced heating (n = 3). Data are mean ± SD from three biologically independent replicates; one-way ANOVA: $^{**}p < 0.01$, ns, not significant.

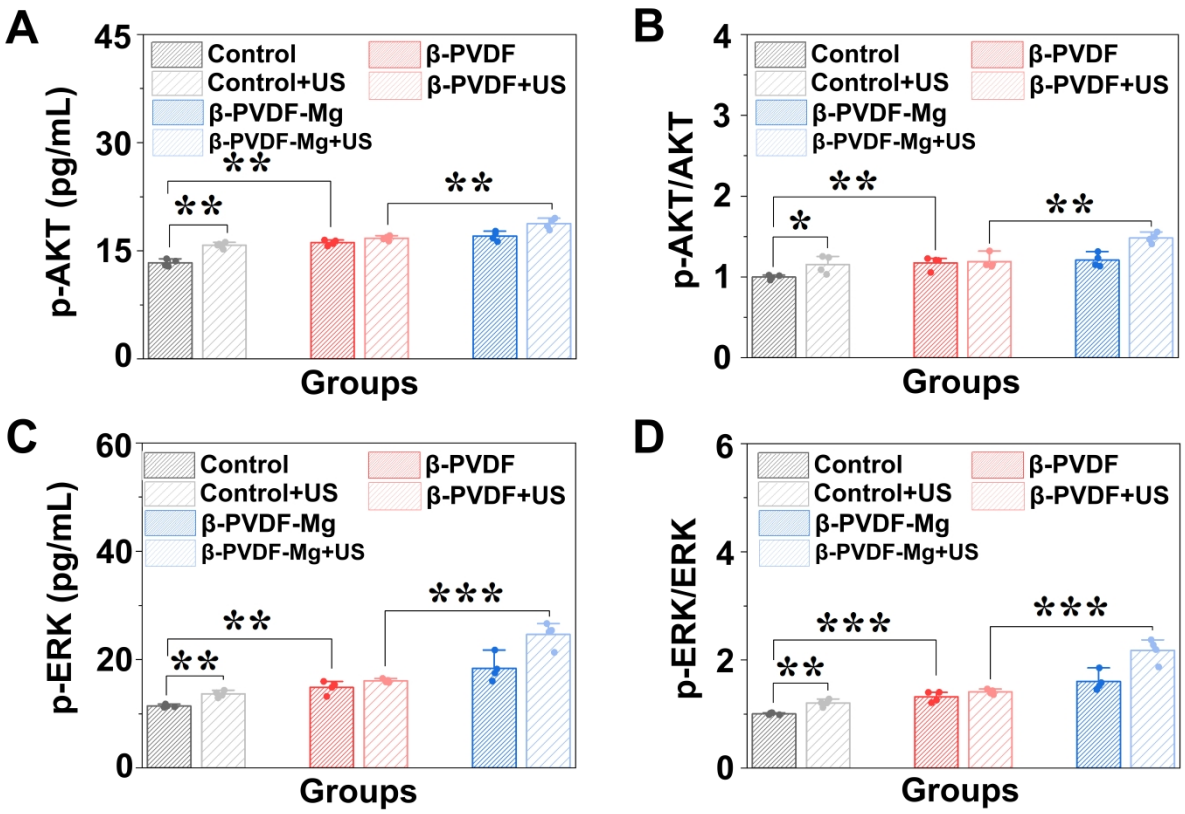


Figure S11. Phosphorylation-level validation of AKT and ERK signaling in RAW264.7 macrophages. (A-B) Quantification of the p-AKT and p-AKT/AKT ratio. **(C-D)** Quantification of the p-ERK and p-ERK/ERK ratio determined by phosphorylation-specific ELISA (n = 4). Data are shown as mean ± SD from four biologically independent replicates; one-way ANOVA: *$p < 0.05$, **$p < 0.01$, ***$p < 0.001$.

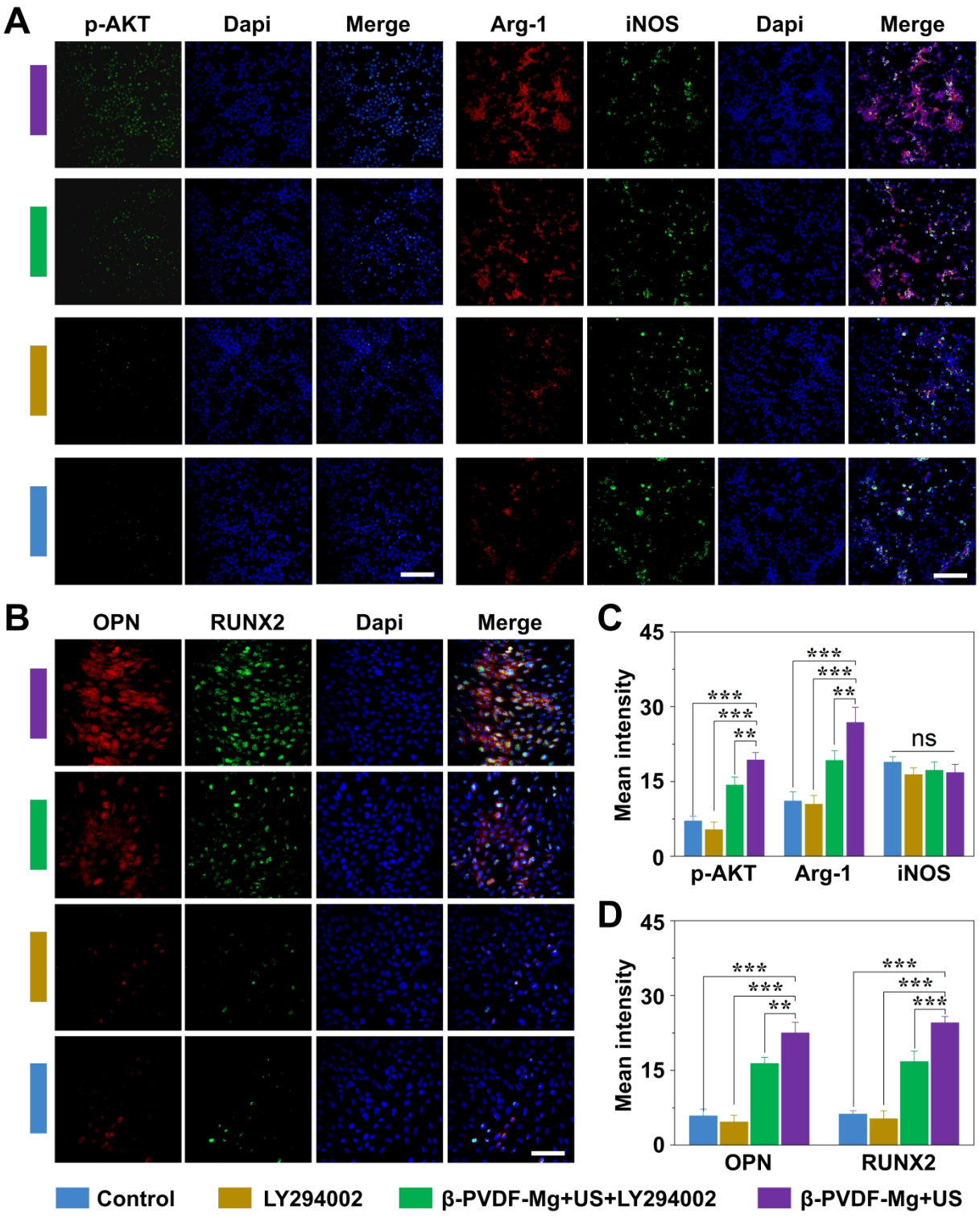


Figure S12. Pharmacological inhibition of PI3K-AKT signaling attenuates β-PVDF-Mg+US-induced reparative macrophage polarization and downstream pro-osteogenic paracrine effects. (A, C) IF staining and analysis of p-AKT, Arg-1 and iNOS in RAW264.7

macrophages (n = 3); scale bar: 100 μm. **(B, D)** Representative IF staining and quantification of RUNX2 and OPN levels in MC3T3-E1 treated with macrophage-conditioned media (n = 3); scale bar: 100 μm. Data are shown as mean ± SD from three biologically independent replicates; one-way ANOVA: $^{**}p < 0.01$, $^{***}p < 0.001$; ns, not significant.

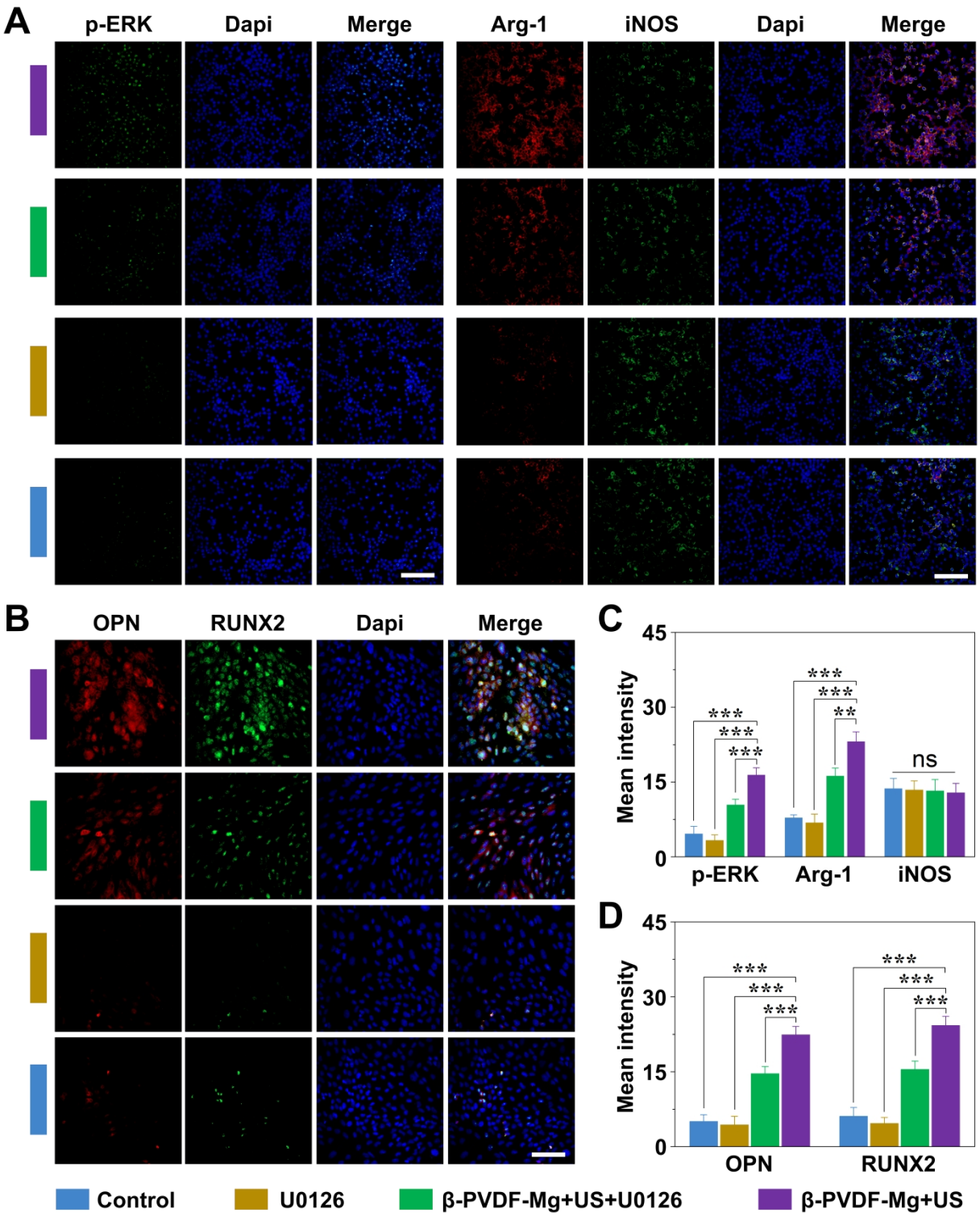


Figure S13. Pharmacological inhibition of MAPK-ERK signaling attenuates β-PVDF-Mg+US-induced reparative macrophage polarization and downstream pro-osteogenic

paracrine effects. (A, C) IF staining and analysis of p-ERK, Arg-1 and iNOS in RAW264.7 macrophages (n = 3); scale bar: 100 μm. **(B, D)** Representative IF staining and quantification of RUNX2 and OPN levels in MC3T3-E1 treated with macrophage-conditioned media (n = 3); scale bar: 100 μm. Data are shown as mean ± SD from three biologically independent replicates; one-way ANOVA: ***$p < 0.001$; ns, not significant.

Table S1. Primers used for RT-qPCR

Gene name	Sequences (5'-3')
P53	*F: CAGCACATGACGGAGGTTGT*
	R: TCATCCAAATACTCCACACGC
Igf1	*F: CCTGCACTGGCTGGAATGAG*
	R: CAGTGGTCTTGGGCATGTCA
MMP9	*F: TGAGTCCGGCAGACAATCCT*
	R: CCACGTGCGGGCAGTAA
Col- I	*F: ACGCCATCAAGGTCTACTGC*
	R: ACTCGAACGGGAATCCATCG
ALP	*F: CTGGACTTGGTGGTCACAGC*
	R: CGGGACGAGGAAACACTCTC
Runx2	*F: CGCCTCACAAACAACCACAG*
	R: TGCTTGCAGCCTTAAATATTCCTG
Dusp5	*F: TCTGGACACGGAGGTGGA*
	R: GGTGTTGGTGGTGTTGATGAG
Il1rn	*F: CCTGGTTTCCAGGAAAGTCG*
	R: GCCATTGCTGTAGTGGTCTT
Col5a3	*F: GAGGCTGGAGACCAAGGAAC*
	R: CGGTAGCCACAGAGGTCTTC
P3h2	*F: TGCTGGACCTGGTCAACTAC*
	R: TGGGTCACAGAGGTGTTGAG
GAPDH	*F: AAGAGGGATGCTGCCCTTAC*
	R: CGGGACGAGGAAACACTCTC
Cxcr3	*F: GCTGTCATTGCTGGTGTCTG*
	R: CACAGGGTAGGGTTGCTGAT

Il-1a	*F: GCAACTGTTCCTGAACTCAACT* *R: ATCTTTTGGGGTCCGTCAACT*
Ank	*F: CCGCTACCTCACCAAGATCC* *R: TCCAGCCAGGTCCATCTCTA*
Nfatc1	*F: TGCTCCTCCTCCTGCTGTT* *R: GCTGCCTTCCGTCTCATAGTT*
Acp5	*F: TGTGGCCATCTTTATGCT* *R: GTCATTTCTTTGGGGATT*

Table S2. Comparison of the present strategy with representative piezoelectric biomaterials

Representative study	Wang et al. Bioactive Materials, 2026, 61, 743–757	Liu et al. Biomaterials 2026, 329, 123938	Zeng et al. Regenerative Biomaterials, 2026	Lu et al. Dental Research, 2026, 100044	Yin et al. Bioactive Materials, 2026, 63	This work
Piezoelectric stimulation	✓	✓	✓	✓	✗	✓
Bioactive ion	Mg^{2+}	✗	Ca^{2+} /Si	Drug bioactive molecules	Multiple therapeutic agents	Mg^{2+}
Ion release mode	Sustained degradation-mediated release	—	Sustained release	US-triggered release	NIR-programmable sequential release	US-programmable piezoelectric-regulated release
Surface topography	✗	Partial	Fibrous ECM-like structure	✗	Biomimetic periosteum	Micro/nano linear topology
External regulation	✗	Mechanical/self-powered	✗	US-triggered release	Near-infrared light	US
Unique limitation of previous work / Advantage of this work	Passive Mg^{2+} release without external regulation.	Electrical stimulation only.	Bioactive ion release but no Mg^{2+}-mediated immunomodulation.	US-responsive but without piezoelectric-regulated Mg^{2+} release.	Programmable therapy but without piezoelectric stimulation or Mg^{2+}-mediated osteoimmunomodulation.	US-triggered, externally adjustable Mg^{2+} release coupled with piezoelectric output and micro/nano topographical guidance, coordinated osteoimmune regulation through coupled topographical, electrical, and ionic cues.

Table S3. Statistics of the topographical parameter of β-PVDF-Mg

Topographical parameter of β-PVDF-Mg	Mean ± SD
Ridge width	400 ± 87 nm
Groove width	350 ± 62 nm
Groove depth	306 ± 59 nm

Table S4. Quantitative analysis of XRD

Parameter	β-PVDF	β-PVDF-Mg	Change
The main peak position of the β phase at 2θ	20.56°	20.60°	+ 0.04°
Original maximum peak intensity	427,487	441,117	+ 3.2%
Peak height after background correction	397,610	412,435	+ 3.7%
FWHM	0.997°	0.969°	− 2.8%
Integrated area of β peak	471,122	477,149	+ 1.3%
β peak area/total XRD integrated area	42.17%	42.92%	+ 0.75 percentage points

Table S5. The residual Mg content of the β-PVDF-Mg patches (8 w)

Samples	Remaining Mg^{2+} content (mmol)	Remaining Mg^{2+} ratio (%)
Initial β-PVDF-Mg patch	0.05 ± 0.003	1
β-PVDF-Mg after 8 weeks *in vivo* without US	0.041 ± 0.006	82
β-PVDF-Mg after 8 weeks *in vivo* with US	0.004 ± 0.00035	8

Table S6. Experimental group definitions and corresponding material characteristics and treatments

Group	Materials	Morphology	Polarization	Mg	US
Control	β-PVDF	No	Yes	No	No
Control+US	β-PVDF	No	Yes	No	Yes
β-PVDF	β-PVDF	Yes	Yes	No	No
β-PVDF+US	β-PVDF	Yes	Yes	No	Yes
β-PVDF-Mg	β-PVDF-Mg	Yes	Yes	Yes	No
β-PVDF-Mg+US	β-PVDF-Mg	Yes	Yes	Yes	Yes

Table S7. US average output power conversion table

US output power (W)	Area-averaged acoustic intensity (mW/cm^2)
0.5	25
0.6	30
1	50
2	100
3	150